# TROPOSPHERIC $NO_2$ OVER CHINA

**R.J. van der A[1], D.H.M.U. Peters[1,2], J.J.P. Kuenen[1,2], H.J. Eskes[1], K.F. Boersma[1], M. Van Roozendael[3], I. De Smedt[3], P.Zhang[4], H.M. Kelder[1,2]**

[1] *Royal Netherlands Meteorological Institute, The Netherlands*
[2] *Eindhoven University of Technology, The Netherlands*
[3] *Belgian Institute For Space Aeronomy, Belgium*
[4] *National Satellite Meteorological Center, Chinese Meteorological Administration, Beijing*

## ABSTRACT

The results are presented of a study to tropospheric $NO_2$ over China, based on measurements from the satellite instruments GOME and SCIAMACHY. A data set of 10 year tropospheric $NO_2$ has been processed from GOME and SCIAMACHY observations using a combined retrieval/assimilation approach. This approach allows the retrieval of global, accurate tropospheric concentrations and detailed error estimates. The resulting dataset has been analysed with statistical methods to derive trends in $NO_2$ and the seasonal variability on a grid of 1x1 degree for all regions of China. The variance and the autocorrelation of the noise are used to calculate the significance of the trend. The results show a large growth of tropospheric $NO_2$ over eastern China, especially above the industrial areas with a fast economical growth. The seasonal pattern of the $NO_2$ concentration shows a clear difference between East and West China. This spatial difference correlates with the dominating source of emissions.

## 1. INTRODUCTION

Nitrogen oxides ($NO_x$=NO + $NO_2$) play an important role in atmospheric chemistry. $NO_x$ has significant natural sources (e.g. lighting and soil emissions) and anthropogenic (e.g. biomass burning, fossil fuel combustion) sources. Global tropospheric $NO_2$ distributions are measured by the satellite instruments GOME (from 1995-2003) aboard ERS-2, SCIAMACHY (from 2002) aboard Envisat platform and OMI aboard EOS-AURA (from 2004) [Leue et al., 2001, Richter et al., 2005; Martin et al., 2002; Boersma et al., 2004]. In Fig. 1. two examples are shown of $NO_2$ observations over China by both GOME and SCIAMACHY.

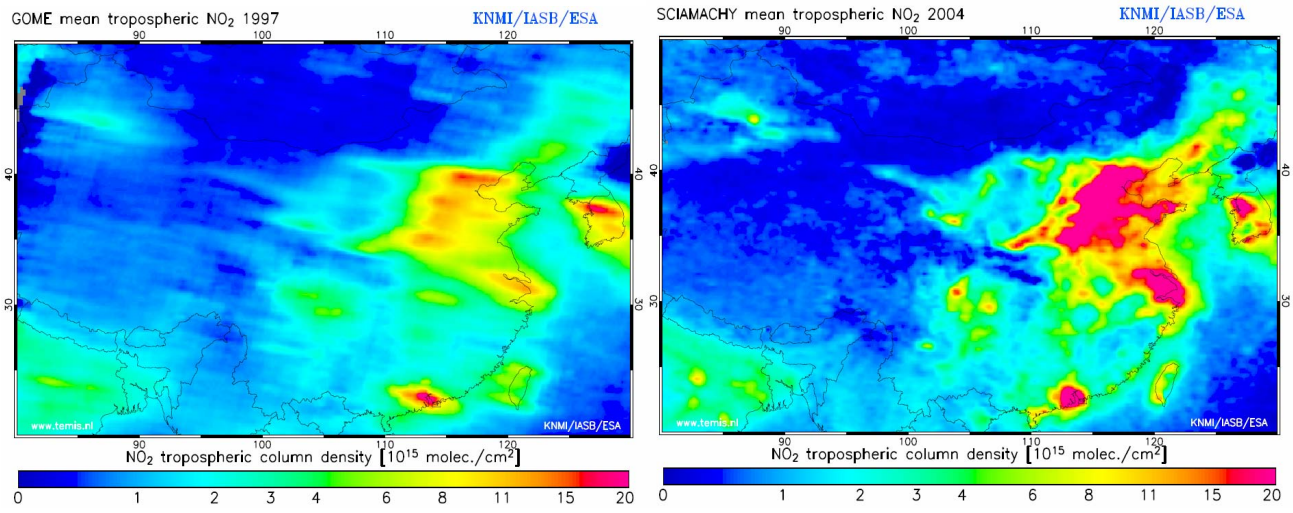


*Fig. 1. Mean tropospheric $NO_2$ as measured by GOME in 1997 (left panel) and by SCIAMACHY in 2004 (right panel). Note the difference in resolution of both instruments but also the increase in measured $NO_2$ in only 7 years time.*

*Proc. 2005 Dragon Symposium "Mid-Term Results", Santorini, Greece*
*27 June – 1 July 2005 (ESA SP-611, January 2006)*

Recent studies on the tropospheric $NO_2$ columns show that the satellite measurements are suitable for improving emission inventories and air quality studies. Jaeglé et al. [2004] used GOME measurements over the Sahel to map the spatial and seasonal variations of $NO_x$, mainly caused by biomass burning and soil emissions. Martin et al. [2003] used GOME measurements to derive a top-down emission inventory. The top-down inventory in combination with bottom-up emission inventory is used to achieve an optimised posterior estimate of the global $NO_x$ emissions. Boersma et al. [2005] used GOME measurements to estimate the global $NO_x$ production from lightning by comparing modelled and measured spatial and temporal patterns of $NO_2$ in the tropics. In Blond et al. [2005] SCIAMACHY measurements are compared with an air quality model and ground measurements. They showed that SCIAMACHY measurements are able to monitor the air pollution over Europe and its day-to-day changes.

In this study we focus on China for the period 1996 to 2004. China has one of today's fastest growing economies of the world. This increase in economical activity is accompanied by a strong increase of emissions of tropospheric pollutants and therefore leads to extra pressure on the environment. We will combine GOME and SCIAMACHY measurements to obtain a 9-year dataset that is suitable for a trend study. The strong increase in $NO_x$ emissions in China is due to a increase in industry and traffic, see Wang et al. [2004]. These emissions are concentrated on the densely populated and industrialized eastern part of China, as can be seen in Fig. 2.

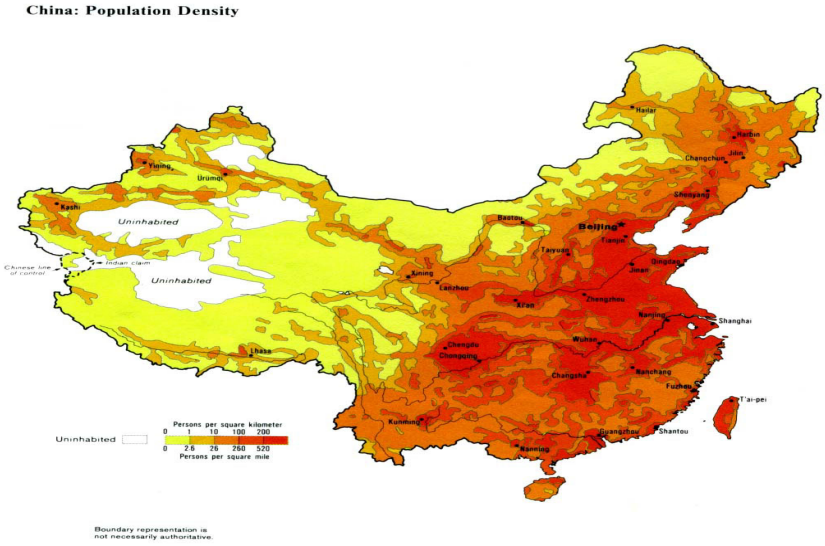


*Fig. 2. The population density in China. The red areas in East China are the major industrial and urbanized regions of China. (Courtesy of the University of Texas Libraries, The University of Texas at Austin.)*

The combination of the variability in both chemistry and emissions leads to a seasonally dependent $NO_2$ concentration with an expected maximum of $NO_2$ in wintertime. The $NO_2$ lifetime is in the order of one day depending on many factors like meteorological conditions, photolysis time scale and OH concentrations. A higher actinic flux results in a higher OH concentration (if the water vapor concentration is high enough), which reacts with $NO_2$ to form $HNO_3$, the principal sink for $NO_x$. The emissions also show variability.

## 2 Tropospheric $NO_2$ retrieval

The GOME and SCIAMACHY spectrometers measure backscattered light from the Earth in the UV and visible wavelength range. From the observed spectral features around 425-450 nm slant column densities (SCD) of $NO_2$ are derived with the Differential Optical Absorption Spectroscopy (DOAS) method [Platt, 1994]. The work presented here is based on slant columns retrieved from the satellite data by BIRA-IASB [Vandaele et al., 2005]. The $NO_2$ stratospheric column is deduced

from a chemistry-transport model assimilation run of the $NO_2$ slant column data. Subsequently, the assimilated stratospheric slant column is subtracted from the retrieved DOAS total slant column, resulting in a tropospheric slant column. The tropospheric NO2 columns are derived from these slant columns [Boersma et al., 2004]. Height-dependent air mass factor (AMF) lookup tables are based on calculations with the Doubling-Adding KNMI (DAK) radiative transfer model. The tropospheric vertical column is retrieved using TM4 [Dentener et al., 2003] tropospheric model profiles (co-located for each GOME and SCIAMACHY pixel individually) and combined with albedo and cloud information. The latter consists of cloud fraction and cloud top height derived by the FRESCO algorithm [Koelemeijer et al., 2003]. Only observations with an estimated cloud radiance of less than 0.5 are used in this study. The retrieval includes surface albedo values constructed from a combination of the TOMS-Herman-Celarier-1997 and Koelemeijer-2003 surface reflectivity maps (available on a monthly basis). No aerosol correction is applied. This choice is based on the realization that the cloud retrieval will be influenced by aerosol as well, and is further motivated by the error analysis presented in the work of Boersma et al. [2004]. The final $NO_2$ column data product is publicly available on the TEMIS project website (www.temis.nl) with detailed error estimates and kernel information [Eskes and Boersma, 2003]. In Fig. 3 the year average tropospheric $NO_2$ column of 2004 is given. The Figure shows high concentration above the highly populated regions like Beijing, Shanghai, Hong Kong and South Korea. It can also be seen that the satellite is detecting the emissions around the Yellow river (Huang He). Over western China, low $NO_2$ columns are observed except over the large city Urumqi in the Northwest.

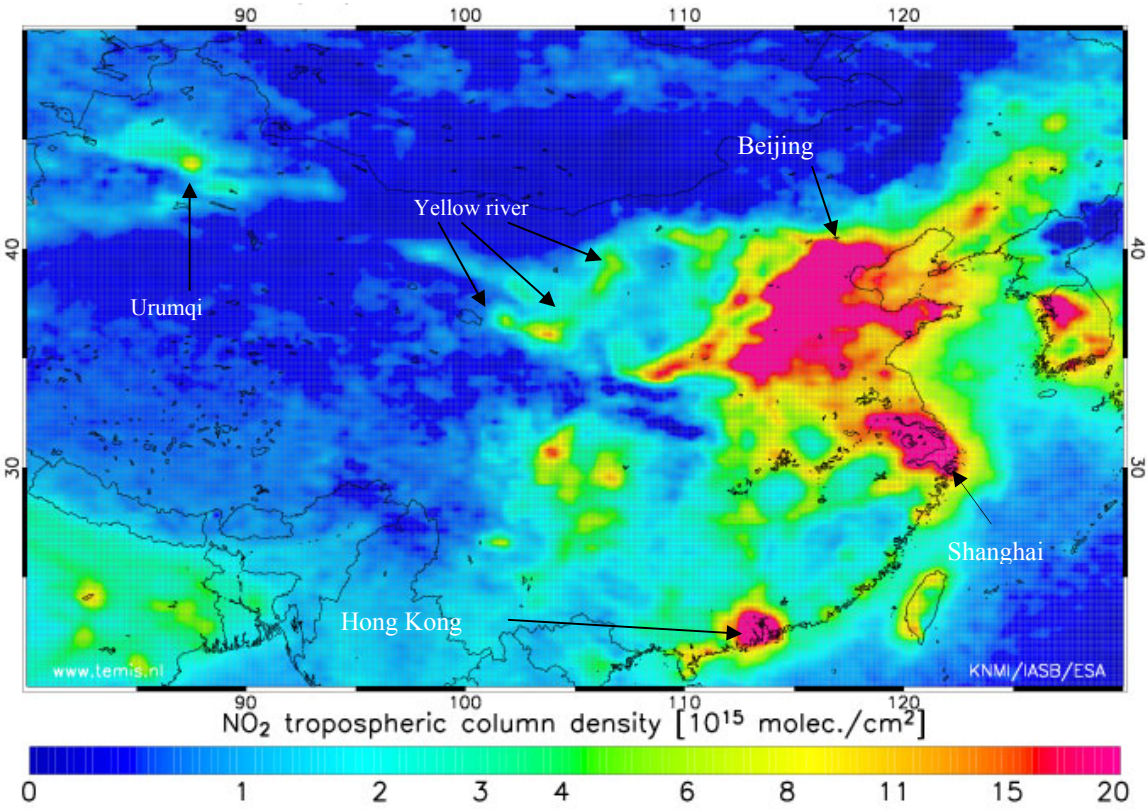


*Fig. 3. The yearly averaged tropospheric $NO_2$ column measured by SCIAMACHY for 2004.*

## 3 Data analysis

The GOME data from March 1996 till March 2003 and the SCIAMACHY data from April 2003 till December 2004 have been used to analyze the trends and variability in $NO_2$ over China. April 2003 is the first month where SCIAMACHY $NO_2$ columns are retrieved successfully. The retrieved tropospheric $NO_2$ columns are gridded on a 1° by 1° grid, using weighting factors for the overlap between satellite pixel and grid cell. The 1 by 1 grid is chosen to average out the effect of different satellite pixel sizes.

For each cell two time series are determined; a time series based on a two weeks average and one based on a monthly average. Both time series are tested for the best fit. Because of the larger sample the monthly average lead to a better and more consistent time series. The negligible weekly cycle of the $NO_2$ concentration above China makes it unnecessary to compensate for lower weekend measurements.

The temporal variability in the $NO_2$ columns is usually larger than the precision of the measurements. To account for both effects, the uncertainty of the monthly mean is determined by taking the sample standard deviation of the mean. The measurement error on the tropospheric $NO_2$ for individual pixels as calculated by [Boersma et al.,2004] shows a dependency on the absolute value of tropospheric $NO_2$, having a minimum error of about $1 \cdot 10^{15}$ molec/cm$^2$. This minimum error is used as lower limit for the error on the monthly average $NO_2$ concentration to avoid a non-realistic accuracy caused by a limited number of samples.

Two models have been used to fit the time series, a model with a linear trend and a seasonal component for the annual cycle of $NO_2$, and a model with an exponential trend. The model with the linear trend is described by the following function based on Wheaterhead et al. [1998],

$$Y_t = A + BX_t + C\sin(DX_t + E) + \delta U_t + N_t, \qquad (1)$$

where $Y_t$ represents the monthly $NO_2$ column of month $t$ and $X_t$ is the number of months after January 1996, $N_t$ is the remainder (residual unexplained by the fit function) and $A,B,C,D,E,\delta$ are the fit parameters. Parameter $A$ represents the $NO_2$ column in January 1996, and $B$ is the monthly trend in $NO_2$. The seasonal component contains amplitude $C$, a frequency $D$ and a phase shift $E$. The fit of the frequency $D$ leads to an expected period of one year, therefore this fit parameter was fixed for the final analyses. The data has also been fitted with a linear model, without a seasonal component. The analyses of this fit showed that the seasonal component was an essential part of the model. A linear growth was used to fit the time series since there is no large distinction between a linear and an exponential growth of the tropospheric $NO_2$ column over China in the period 1996 to 2004.

The term $\delta U$ in Eq. 1 is used to fit the bias between the measurements of GOME and SCIAMACHY, where $\delta$ is the value of the bias and $U_t$ is,

$$U_t = \begin{cases} 0 & t < T_0 \\ 1 & t \geq T_0 \end{cases}. \qquad (2)$$

In this Eq. 2 the time $T_0$ ($0 < T_0 < T$) is the moment when the time series switches from using GOME to using SCIAMACHY data, which in this case is April 2003. The total number of months is denoted by $T$. The bias $\delta$ is fitted and checked for latitude dependence over China. We find that the bias is negligible, with values less than 0.01 $10^{15}$ molec/cm$^2$. Based on this result the bias term is set to zero in analysis below.

The remainder, $N_t$ in Eq. 1 is the difference between the model and the measured value. Weatherhead et al. [1998] suggest modeling the remainder by

$$N_t = \phi N_{t-1} + \varepsilon_t, \qquad (3)$$

where $\varepsilon_t$ is the white noise and $\phi$ is the autocorrelation in the remainder. The autocorrelation in the remainder is a result from processes which are persistent with time and which are not described by the fit function, see Tiao et al. [1990]. We produced plots of the correlation between remainders as a function of the time difference. A typical autocorrelation of 0.1 is

found, indicating that the remainders are only weakly correlated. The autocorrelation in the remainder affects the precision of the trend. In Wheaterhead et al. [1998] a derivation is given for the precision of the trend as function of the autocorrelation, the length $T$ of the dataset in months and the variance in the remainder, $\sigma_N$.

The length of the dataset in years, $n$, is introduced to express the precision of the trend per year. For small autocorrelations the standard deviation $\sigma_B$ of the trend per year is approximately given by

$$\sigma_B \approx \left[ \frac{\sigma_N}{n^{3/2}} \sqrt{\frac{1+\phi}{1-\phi}} \right]. \qquad (4)$$

## 4 Trends in tropospheric NO2

For each grid cell in China the model following Eq. 1, is applied, leading to a spatial distribution of each of the fitting parameters of the model. In Fig. 5 the trend in $NO_2$ concentration is, shown as the yearly increase in tropospheric $NO_2$. The trend is the highest in the eastern part of China, corresponding to the regions with a fast industrial and economical development. The fastest growing economy is in the Shanghai region, which also shows the largest growth of tropospheric $NO_2$. It is interesting to note that the growth in the region around Hong Kong is less than for other regions with a high economical activity. This is probably due to the already high level of economic activity in 1996 when our trend study started and a package of measures against air pollution in Hong Kong over the last years.

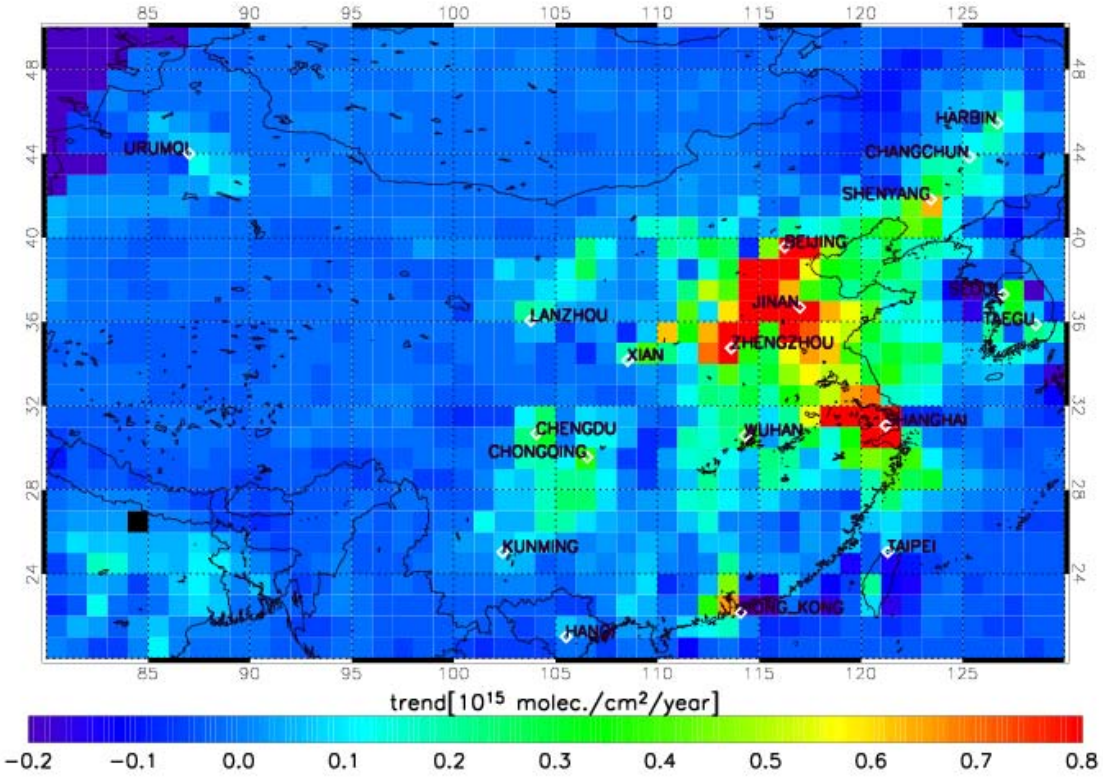


*Fig. 4. The trend of the $NO_2$ concentration over China for the period 1996-2004.*

The precision $\sigma_B$ of the trend on $NO_2$ is calculated using Eq. 4. In Fig. 4 the trend divided by the precision is shown. It is a common decision rule for trend detection that a trend $B$ is real with a 95% confidence level if $|B/\sigma_B| > 2$ [Wheaterhead et al.,

1998]. Fig. 5 shows that a significant trend (white grid cells) is detected in the regions of East China with a high population and high industrial activity. From Eq. 4 can be seen that the standard deviation of the trend decreases if the length of the dataset increases. Therefore, it can be expected that for more grid cells a significant trend can be detected with a longer dataset.

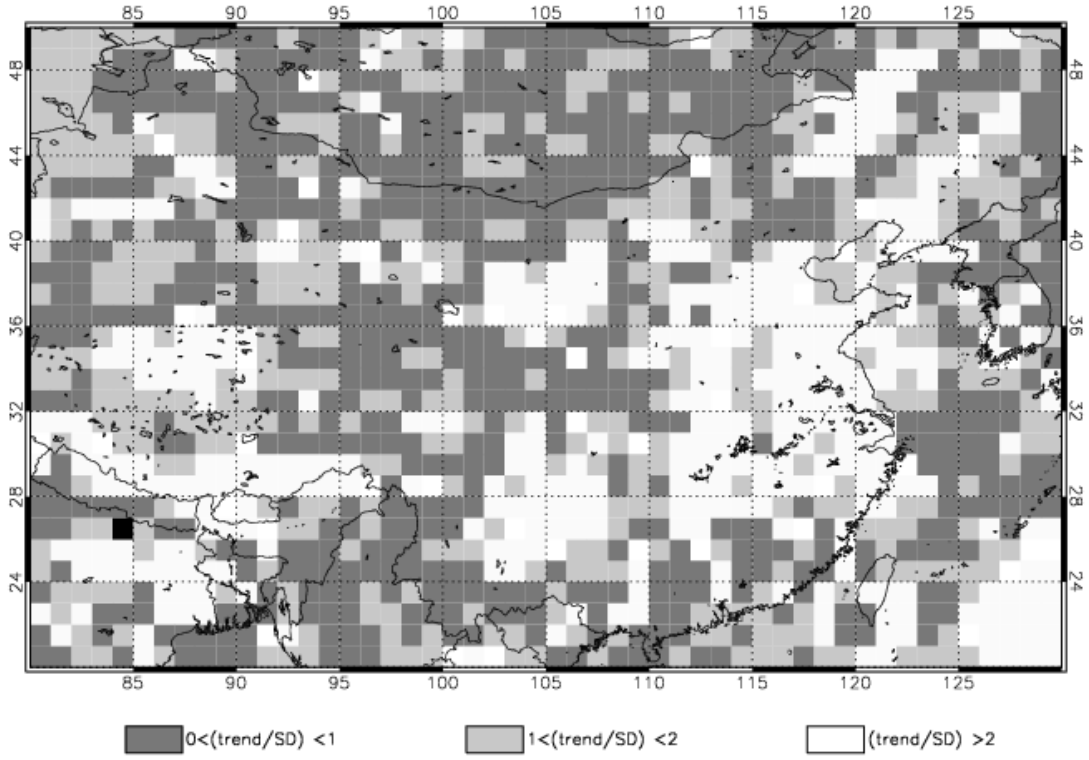


*Fig. 5. The $NO_2$ trend per year divided by the standard deviation. If this value is higher than 2 (white areas) a real trend is indicated with a 95% confidence level.*

In Table 1 the trend estimates and start values for some major cities are shown. A yearly growth is determined in terms of percentage with respect to the start value in 1996. Shanghai is one of the fastest growing industrial areas, which is reflected in a large growth in $NO_2$. The trend over Taipei is not significant in this period. This is probably due to the effect of measures by the government to improve the air quality in Taiwan (These measures included subsidies on environmental-friendly techniques in traffic, improved public transport, and imposing pollution penalties)

*Table 1. The observed trends for some cities in East Asia. The percentage is calculated with respect to the year 1996.*

| | $NO_2$ concentration in January 1996 [$10^{15}$ molec/cm$^2$] | Linear trend in $NO_2$ [$10^{15}$ molec/cm$^2$/ year] | Error on trend [$10^{15}$ molec/cm$^2$/year] | Growth (reference year 1996) |
|---|---|---|---|---|
| Hong Kong | 7.63 | 0.72 | 0.48 | 8% |
| Beijing | 10.92 | 1.20 | 0.48 | 11% |
| Shanghai | 5.48 | 1.44 | 0.35 | 25% |
| Taipei | 4.89 | -0.02 | 0.06 | 0% |
| Chongqing | 3.10 | 0.40 | 0.10 | 13% |
| Seoul | 9.95 | 0.36 | 0.21 | 4% |
| Background (86°E x 40°N) | 0.5 | 0 | 0.01 | 0% |

## 5 The relation between tropospheric $NO_2$ columns and $NO_x$ emissions

To see how a change in $NO_x$ tropospheric column density is related to a change in $NO_x$ emissions, the effect of doubling the anthropogenic emissions on the $NO_x$ tropospheric column density has been studied. Using the chemistry-transport zoom model TM5 (Krol et al., 2005) with zooming on China, tropospheric $NO_x$ columns can be determined on a 1x1 degree resolution for China. In Fig. 6 the ratio between two tropospheric columns is plotted; one with regular emissions and one where the anthropogenic emissions are doubled. This factor 2 has been chosen, because it is a typical increase in $NO_2$ tropospheric column over a 10-year period.

From this picture it can be concluded that in places where very little anthropogenic $NO_x$ emissions are present (like in West China), the ratio is close to 1, as expected. In places with high anthropogenic $NO_x$ emissions however, doubling the $NO_x$ emissions means that the $NO_x$ tropospheric column density becomes nearly twice as large. The highest values typically occur in the places with the highest tropospheric $NO_2$ column density, the anthropogenic $NO_x$ emissions are predominant here.
The ratio between the tropospheric column densities does not exceed the factor 2, which means that the trend in tropospheric $NO_x$ column is a minimum for the trend in $NO_x$ emissions.

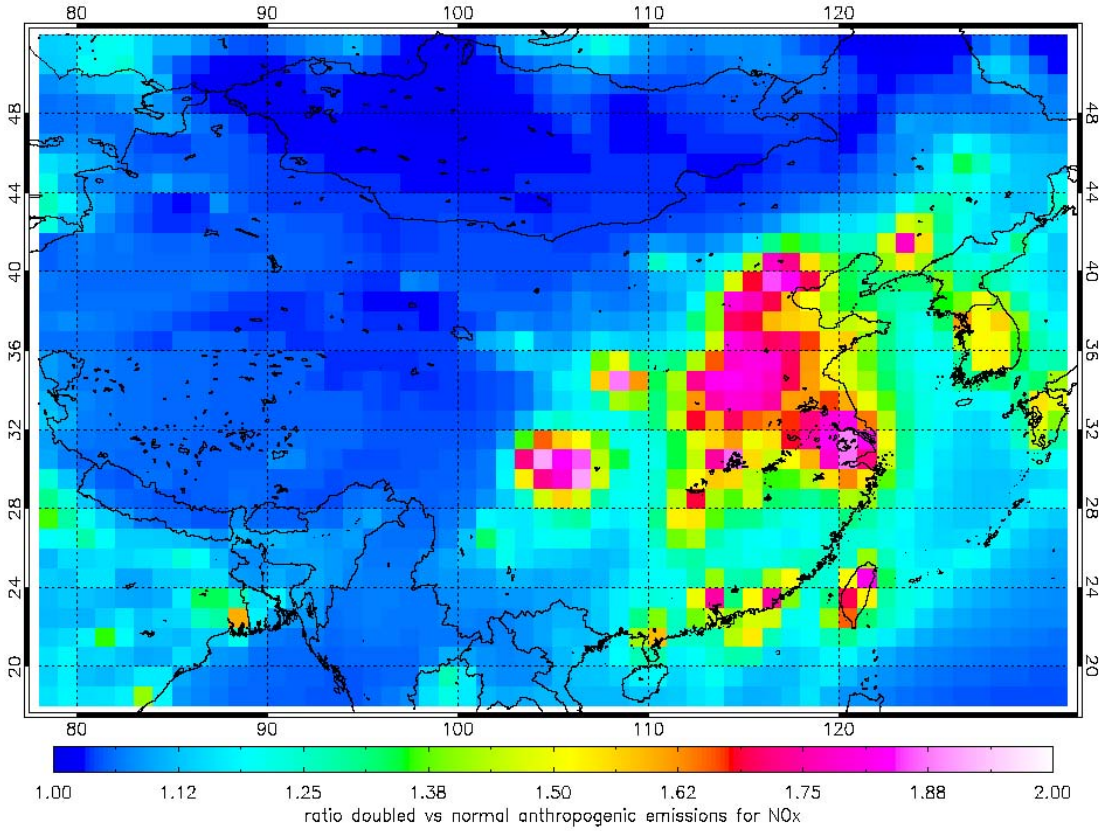


*Fig. 6. Map of ratios between tropospheric $NO_x$ columns modelled with standard emissions and modelled with doubled anthropogenic emissions. The model runs are performed for the annual average of 2001.*

## 6 The $NO_2$ seasonal cycle

The time series of $NO_2$ usually show a strong seasonal cycle, which has also been fitted using Eq. 1 allowing us to study the seasonal cycle of the $NO_2$ concentration. Since the lifetime of $NO_x$ is longer in wintertime, a $NO_2$ maximum is expected in the winter. Fig. 7 shows that the month with the largest $NO_2$ abundances in the East and South of China is according to the expected winter maximum, but in the West a $NO_2$ maximum during summertime is found. The black grid cells correspond to regions where a linear fit works just as well but without a clear seasonal cycle.

The western part of China has a low population density (see Fig. 2). As a consequence natural emissions are expected to dominate the tropospheric column. Fig. 6 shows that in the North West, above the large city Urumqi, a winter maximum is found, which strengthens the idea that the summer maximum in $NO_2$ over the rest of West China is caused by natural emissions.

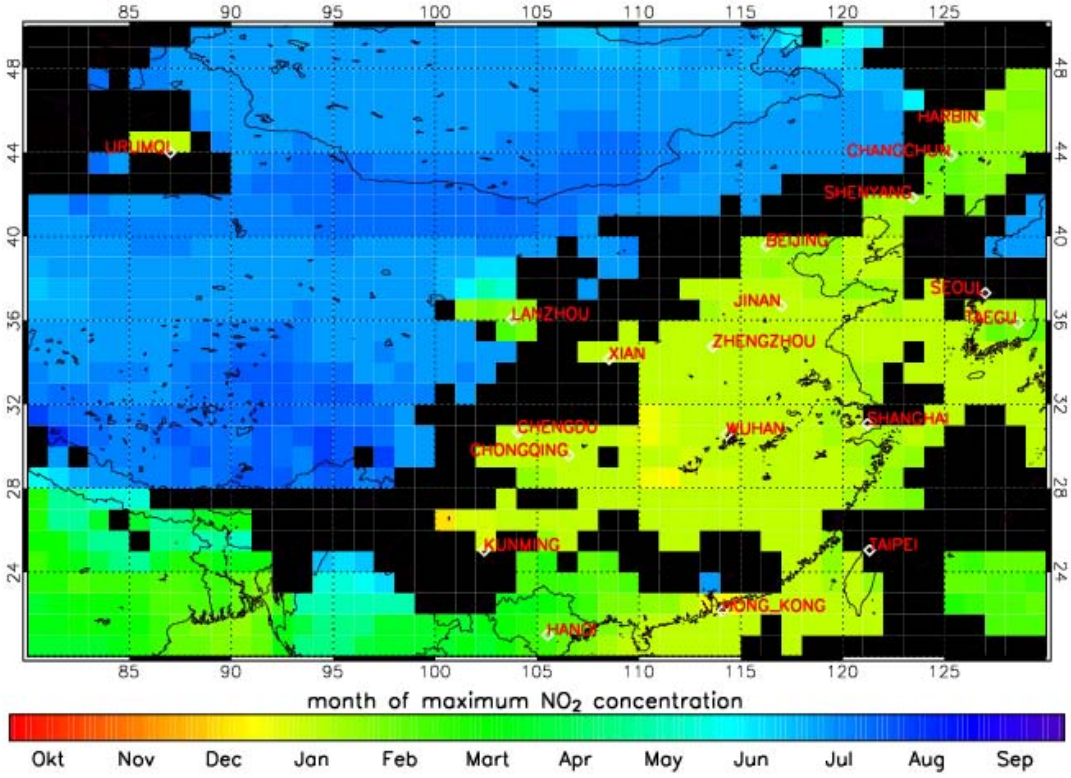


*Fig. 7. Map of China showing the month where the yearly seasonal component has its maximum in $NO_2$ concentration. In East China a maximum is found during the winter and in the West of China a maximum is found during the summer. The black pixels are regions where a linear fit without a seasonal component is more accurate.*

Lightning flash densities are measured by the Optical Transient Detector (http://thunder.msfc.nasa.gov/OTDsummaries). From a comparison between the summer and winter flash densities can be concluded that lightning above China especially occurs during summertime. The contribution of lightning to the tropospheric $NO_2$ column is strongest in the tropics, with an estimated maximum of 0.4 $10^{15}$ molec/cm$^2$ [Edwards et al., 2003, Boersma et al., 2005]. Because the difference between summer and winter tropospheric columns is typical of the order 1.0 $10^{15}$ molec/cm$^2$, lightning alone cannot account for all the natural emissions in West China. Bryan et al. [2003] show that there is no biomass burning in the western part of China.

In Yienger et al. [1995] it is suggested that in remote agriculture regions soil emissions contribute 50% to the total $NO_x$ budget and that in July these percentages can rise to more than 75%. Yienger et al. [1995] also suggested that soil $NO_x$ emissions are temperature dependent, soil dependent and precipitation dependent. A higher surface temperature leads to more $NO_x$ emissions, which would explain higher $NO_x$ concentrations in summer time. They also found higher $NO_x$ emissions for grassland that together with desert and scrub land form the main soil composition in West China. Another effect that increases soil $NO_x$ emissions in summertime is "pulsing", which is described in [Yienger et al., 1995] and [Jaeglé et al., 2004] as an increase in $NO_x$ measured after a shower of rain. From the IRI/LDEO Climate Data library it can be seen that in the West part of China it is only raining in the summer season. This also contributes to enhanced $NO_2$ concentrations during summertime.

## 7 Conclusions

The tropospheric $NO_2$ columns measured by GOME and SCIAMACHY have been used for trend analysis over China. A linear model with a seasonal component is used to fit the time series of $NO_2$ concentrations. By applying this model to each grid cell a spatial distribution of the fit parameters is calculated. Furthermore the precision of the trend is calculated.

It can be concluded that the 9 years long $NO_2$ dataset from GOME and SCIAMACHY can be used for trend analysis in the eastern part of China. In this highly populated and industrialised area the trend is large enough to be significant. For instance Shanghai had a yearly increase of 25% in 1996. For other regions longer time series are needed to detect a significant signal.

The geographic distribution of the seasonal cycle of tropospheric $NO_2$ was studied. In the eastern part of China an expected winter maximum is found. In the western part of China this cycle shows a $NO_2$ maximum in summer time. As there is nearly no anthropogenic activity in Western China, this cycle is attributed to natural emissions, especially soil emissions and lightning.

The bias between the monthly GOME and SCIAMACHY tropospheric $NO_2$ series appears to be negligible and does not show any latitude dependence. This shows the consistency in the retrieval method of tropospheric $NO_2$ and allows the use of long time series by combining different instruments to detect a significant trend for regions without a large trend.

It is well known that emissions are increasing over China [Streets et al., 2003; Wang et al., 2004]; this study shows that the satellite measurements are able to measure the increase of atmospheric concentrations. Our first results from modelling studies indicate that the trends found in the satellite observations of $NO_2$ can be considered lower boundaries of the actual trends in emissions of $NO_x$.

## References


Blond, N., K.F. Boersma, H.J. Eskes, R.J. van der A, M. Van Roozendael, I. De Smedt, G. Bergametti, and R. Vautard (2005), Intercomparison of SCIAMACHY nitrogen dioxide observations, in-situ measurements, and air quality modeling results over Western Europe, submitted to *J. Geophys. Res*

Boersma, K.F., H.J. Eskes and E.J. Brinksma (2004), Error analysis for tropospheric NO2 retrieval from space, *J. Geophys. Res.*, *109*(D0) ,4311, doi: 10.1029/2003JD003961.

Boersma, K.F., H.J. Eskes, E.W. Meijer, and H.M. Kelder (2005), Estimates of lightning $NO_x$ production from GOME satellite observations, *Atmos. Chem. Phys. Discuss,* 5, 3047-3104

Boersma, K.F.(2005), Satellite observations of tropospheric nitrogen dioxide; retrieval interpretation and modelling, Ph.D Thesis, Universiteitsdrukkerij Technische Universiteit Eindhoven, Eindhoven

Bryan N. D., R.V. Martin, A.C. Staaudt, R.Yevich, and J.A. Logan. (2003),Interannual and seasonal variability of biomass burning emissions constrained by satellite observations, J. *Geophys. Res*., *108* (D2), 4100, doi:10.1029/2002/JD002378

Dentener, F.,M. van Weele, M. Krol, S Houweling, and P. van Velthoven (2003), Trends and inter-annual variability of methane emissions derived from 1979-1993 global ctm simulations, *Atmos. Chem. Phys., 3,* 73-88

Edwards, D. P., J.F. Lamarque, J.L, Attie, L. K. Emmons, A. Richter, J.P. Cammas, J. C. Gille, G. L. Francis, M. N. Deeter, J. Warner, D. C. Ziskin, L. V. Lyjak, J. R. Drummond, and J. P. Burrows (2003), Tropospheric Ozone Over the Tropical Atlantic: A Satellite Perspective, *J. Geophys. Res*, *108*(D8), 4237, doi:10.1029/2002JD002927,

Eskes, H. and F. Boersma (2003), Averaging Kernels for DOAS total-column satellite retrievals. *Atmos Chem. Phys*., *3*, 1285 – 1291, 2003

Jaeglé, L., R.V.Martin, K.Chance, L.Steinberger, T.P. Kurosu, D.J. Jacob, A.I.Modi, V.Yoboué, L. Sigha-Nkamdjou, and C.Galy-lacaux (2004), Satellite mapping of rain-induced nitric oxide emissions from soils, *J. Geophysical. Res. 109*(D2), 1310, doi:10.1029/2004JD004787

Koelemeijer, R.B.A., J.F. de Haan, and P. Stammes (2003), A database of spectral surface reflectivity in the range 335-772 nm derived from 5.5 years of GOME observations, *J. Geophys. Res.,108*(D2), doi: 10.1029/2002JD002429

Krol, M., S. Houweling, B. Bregman, M. van den Broek, A. Segers, P. van Velthoven, W. Peters, F. Dentener and P. Bergamaschi, The two-way nested global chemistry-transport zoom model TM5: algorithm and applications, *Atmos. Chem. Phys*., 5, 417-432, 2005.

Leue, C., M. Wenig, T. Wagner, O. Klimm, U. Platt, and B. Jähne (2001), Quantitative analysis of $NO_x$ emissions from Global Ozone Moinitoring Experiment satellite image sequences, *J. Geophys. Res,106*, 5493-5505

Martin, R.V., K.V. Chance, D.J.Jacob, D.J., Kursou, T.P., Spurr, R.J.D., Bucsela, E., Gleason, J.F., Palmer, P.I., Bey, I., Fiori., A.M., Li, Q. and Koelemeijer, R.B.A.(2002), *An improved retrieval of tropospheric nitrogen dioxide from GOME, J. Geophys. Res,107*(D20)4437, doi:10.10129/2001JD001027

Martin, R.V., D.J. Jacob, K.V. Chance, T.P. Kurosu, P.I. Palmer, and M.J. Evans (2003), Global inventory of Nitrogen Dioxide Emissions Constrained by Space-based Observations of $NO_2$ Columns, *J. Geophys. Res., 108*(D17), 4537, doi:10.1029/2003/JD003453

Richter A., J.P. Burrows, H. Nüβ, C. Granier, U. Niemeier, Increase in tropospheric nitrogen dioxide over China observed from space, Nature, 437, 129-132, doi: 10.1038/nature04092, 2005.

Platt, U.(1994), Differential Optical Absorption Spectroscopy (DOAS), in *Air Monitoring by Spectroscopic Techniques, Chem. Anal., vol. 127, edited by M.W. Sigrist, pp. 27-76, Wiley-Interscience, Hoboken, N.J.*

Streets, D.G., T.C. Bond, G.R. Carmichael, S.D. Fernandes, Q. Fu, D. He, Z. Klimont, S.M. Nelson, N.Y. Tsai, M.Q. Wang, J.-H. Woo, and K.F. Yarber (2003), An inventory of gaseous and primary aerosol emissions in Asia in the year 2000 *J. Geophys. Res., 108*(D21), 8809, doi:10.1029/2002JD003093

Tiao, G.C. Reinsel, Daming XU, J.H. Pedrick, Xiaodong Zhu, A.J. Miller, J.J. DeLuisu, C.L. Mateer, and D.J. Wuebbles (1990), Effects of autocorrelation and temporal sampling schemes on estimates of trend and spatial correlation, *J. Geophys. Res.*, *95*,20.507-20.517

Vandaele, A.C., C. Fayt, F. Hendrick, C. Hermans, F. Humbled, M. Van Roozendael, M. Gil, M. Navarro, O. Puentedura, M. Yela, G. Braathen, K. Stebel, K. Tørnkvist, P. Johnston, K. Kreher, F. Goutail, A. Mieville, J.-P. Pommereau, S. Khaikine, A. Richter, H. Oetjen, F. Wittrock, S. Bugarski, U. Friess, K. Pfeilsticker, R. Sinreich, T. Wagner, G. Corlett, R. Leigh, (2005), An intercomparison campaign of ground-based UV-Visible measurements of $NO_2$, BrO, and OClO slant columns. I. Methods of analysis and results for $NO_2$, *J. Geophys. Res.*, 110, D08305, doi:10.1029/2004JD005423.

Wang, Y. X., and M.B. McElroy (2004), Asian emissions of CO and $NO_x$: Constraints from aircraft and Chinese station data, *J. Geophys. Res*, *109*,(D2),4304, doi:10.1029/2004JD005250.

Weatherhead, E.C., G.C. Reinsel, G.C. Tiao, X. Meng, D. Choi, W. Cheang, T. Keller, J. DeLuisi, D. J. Wuebbles, J.B. Kerr, A.J. Miller, S. J. Oltmans, and J.E. Frederick (1998), Factors affecting the detection of trends: Statistical considerations and applications to environmental data, *J. Geophys. Res*., *103*, 17.149-17.161

Yienger J.J., and H. Levy II(1995), Empirical model of global soil-biogenic $NO_x$ emissions, *J. Geophys. Res.*, *100*, 11.447-11.464